Atmos. Chem. Phys., 18, 327–338, 2018
https://doi.org/10.5194/acp-18-327-2018

Atmospheric Chemistry and Physics
Open Access
EGU

Heterogeneous reaction of HO_2 with airborne TiO_2 particles and its implication for climate change mitigation strategies

Daniel R. Moon[1], Giorgio S. Taverna[2], Clara Anduix-Canto[1], Trevor Ingham[1,3], Martyn P. Chipperfield[2,3], Paul W. Seakins[1,3], Maria-Teresa Baeza-Romero[4], and Dwayne E. Heard[1,3]

[1]School of Chemistry, University of Leeds, Leeds, LS2 9JT, UK
[2]School of Earth and Environment, University of Leeds, LS2 9JT, UK
[3]National Centre for Atmospheric Science, School of Chemistry, University of Leeds, Leeds, LS2 9JT, UK
[4]Escuela de Ingeniería Industrial, Universidad de Castilla – La Mancha, 45071 Toledo, Spain

Correspondence: Dwayne E. Heard (d.e.heard@leeds.ac.uk)

Received: 11 May 2017 – Discussion started: 22 May 2017
Revised: 19 October 2017 – Accepted: 22 October 2017 – Published: 11 January 2018

Abstract. One geoengineering mitigation strategy for global temperature rises resulting from the increased concentrations of greenhouse gases is to inject particles into the stratosphere to scatter solar radiation back to space, with TiO_2 particles emerging as a possible candidate. Uptake coefficients of HO_2, $\gamma(HO_2)$, onto sub-micrometre TiO_2 particles were measured at room temperature and different relative humidities (RHs) using an atmospheric pressure aerosol flow tube coupled to a sensitive HO_2 detector. Values of $\gamma(HO_2)$ increased from 0.021 ± 0.001 to 0.036 ± 0.007 as the RH was increased from 11 to 66 %, and the increase in $\gamma(HO_2)$ correlated with the number of monolayers of water surrounding the TiO_2 particles. The impact of the uptake of HO_2 onto TiO_2 particles on stratospheric concentrations of HO_2 and O_3 was simulated using the TOMCAT three-dimensional chemical transport model. The model showed that, when injecting the amount of TiO_2 required to achieve the same cooling effect as the Mt Pinatubo eruption, heterogeneous reactions between HO_2 and TiO_2 would have a negligible effect on stratospheric concentrations of HO_2 and O_3.

1 Introduction

It has been suggested that injection of aerosols into the stratosphere in order to scatter solar radiation back to space could be a possible solar radiation management scheme (Shepherd and Working Group on Geoengineering the Climate, 2009). Such a scheme would have the effect of cooling the Earth's surface and serve as a measure to mitigate enhanced global warming. A possible candidate for stratospheric injection is sulfuric acid aerosols as these aerosols occur naturally in the stratosphere. These aerosols are formed by transport of precursors, e.g. SO_2 and carbonyl sulfide (OCS), from the troposphere to the stratosphere (Holloway and Wayne, 2010), which form sulfuric acid vapour that condenses onto particles. However, injection of these particles could have important negative effects on the stratosphere through enhanced ozone depletion. Concentrations of sulfate aerosols can increase dramatically as the result of volcanic eruptions. Following the eruption of Mt Pinatubo in 1991, it was estimated that around 30 Tg of H_2SO_4 was injected in the stratosphere, dramatically increasing stratospheric aerosol loading and hence the available surface area for heterogeneous chemistry to occur (McCormick and Veiga, 1992). Following this volcanic event, the average global lower-tropospheric temperature decreased by 0.5 K (Dutton and Christy, 1992); however, stratospheric ozone concentrations reached a record low in northern mid-latitudes (Dutton and Christy, 1992; McCormick et al., 1995), showing that sulfate aerosols could be unsuitable for solar radiation management. The impact of sulfate geoengineering to stratospheric ozone concentrations is projected to decrease in time as concentrations of Br- and Cl-containing atmospheric species are expected fall, so much so that beyond 2050 the additional available surface area provided by sulfate geoengineering is predicted to enhance conversion of NO_x ($NO_x = NO + NO_2$) to HNO_3, resulting in an increase of stratospheric ozone (Visioni et al.,

2017). Other candidates for particle types, such as TiO_2, have been put forward due to their large refractive indices (Pope et al., 2012), meaning that less stratospheric aerosol loading would be necessary to achieve the same level of cooling. The refractive index of TiO_2 at 550 nm is 2.5 compared to a value of 1.5 for naturally occurring sulfate aerosols (Tang et al., 2014). Assuming that the size of TiO_2 particles can be optimised, it has been reported that, to achieve the same cooling effect that sulfate aerosols had during the Mt Pinatubo event, significantly less TiO_2 than sulfuric acid would be required: approximately 3 times less in mass and 7 times less in volume (Pope et al., 2012). However, the impacts of the presence of TiO_2 particles on stratospheric chemistry have to be determined before this kind of geoengineering solution can be considered. Mineral dust particles are commonly found in the troposphere and contribute the largest fraction to tropospheric aerosol loading in terms of mass (Textor et al., 2006; Huneeus et al., 2011). Typically TiO_2 (which is classified as a mineral) constitutes from 0.1 to 10 % of overall atmospheric mineral dust loading, depending on the location of sources (Usher et al., 2003; Karagulian et al., 2006).

The heterogeneous chemistry of sulfate aerosols in the stratosphere is fairly well understood (Ammann et al., 2013) – for example the conversion of NO_x to nitric acid in the aerosol via N_2O_5 adsorption and reaction, and also the activation of chlorine via the reaction of $ClONO_2$ with HCl to form Cl_2 and nitric acid within cold aerosols. However, the heterogeneous reactivity of mineral particles, in particular TiO_2, is not as well understood. Removal and production of trace gases in the stratosphere may significantly perturb concentrations of O_3; therefore it is important when assessing the potential impact of such a solar radiation management scheme to evaluate the kinetics of likely heterogeneous chemistry.

The hydroperoxyl radical, HO_2, is an important species within the stratosphere, being present at about 5 parts per trillion by volume (pptv) around the tropopause, and is involved in a HO_x catalytic cycle responsible for about 40 % of O_3 depletion in the lower stratosphere via to the following reactions (Wennberg et al., 1994):

$$OH + O_3 \rightarrow HO_2 + O_2 \quad \text{(R1)}$$

$$HO_2 + O_3 \rightarrow OH + 2O_2 \quad \text{(R2)}$$

$$\text{Net}: \ 2O_3 \rightarrow 3O_2.$$

Moreover, HO_2 can also react with stratospheric ClO and BrO to produce HOCl and HOBr respectively, which can be photolysed to produce further OH and atomic halogen species that can contribute to O_3 loss. HO_2 can undergo self-reaction upon surfaces of mineral dust, which is thought to result in the generation of H_2O_2 (Matthews et al., 2014), whose two predominant removal pathways are photolysis and reaction with OH (Versick et al., 2012):

$$H_2O_2 + h\nu(\lambda \leq 360\,\text{nm}) \rightarrow 2OH \quad \text{(R3)}$$

$$H_2O_2 + OH \rightarrow HO_2 + H_2O. \quad \text{(R4)}$$

Although the kinetics of the uptake of HO_2 onto Arizona Test Dust (ATD), a proxy of mineral dust, has been previously investigated (Matthews et al., 2014; Bedjanian et al., 2013), the heterogeneous reaction of HO_2 with TiO_2 has not been studied. However, the kinetics of N_2O_5 uptake (Tang et al., 2014) and $ClONO_2$ (Tang et al., 2016) onto TiO_2 have been studied. The heterogeneous reaction of N_2O_5 results in the conversion to reactive nitrogen oxides (NO and NO_2) involved in a catalytic cycle that leads to significant O_3 depletion and non-reactive HNO_3. The reactive uptake coefficient, γ, which is the probability that a species will collide with an aerosol and be removed by reaction, was measured to be more than an order of magnitude larger for HO_2 onto ATD than for N_2O_5 and $ClONO_2$ onto TiO_2 sub-micron particles, and contrasting dependences of γ with relative humidities (RHs) were observed. Therefore, by analogy it is expected that HO_2 uptake onto TiO_2 may be faster than N_2O_5 uptake. $ClONO_2$ uptake by TiO_2 particles resulted in similar values of γ; however, no dependency of γ with RH between 7 and 33 % was observed.

In this investigation a borosilicate glass aerosol flow tube coupled with a sensitive HO_2 detector based on chemical conversion followed by laser-induced fluorescence detection of OH (George et al., 2013) has been used to study the kinetics of the heterogeneous reaction of HO_2 with airborne TiO_2 nanoparticles at different RH. While it has been possible here to study such kinetics over a range of RHs representative to those typically found in the lower stratosphere (< 40 %) (Wennberg et al., 1994), experimental limitations meant that experiments were only conducted at room temperature (~ 293 K). The TOMCAT three-dimensional (3-D) chemical transport model (CTM; Chipperfield, 1999) has also been used to predict the likely impact of HO_2 uptake by TiO_2 particles on the stratospheric concentrations of HO_2 and O_3.

2 Methods

2.1 Overview of experimental apparatus

The experimental setup deployed for this investigation is similar to other investigations of HO_2 uptake by aerosols undertaken at the University of Leeds (George et al., 2013; Matthews et al., 2014; Lakey et al., 2016); therefore a detailed description of the components of the experiment is not given. A schematic diagram of the experiment is shown in Fig. 1, and all experiments were undertaken at room temperature (293 ± 3 K) and under normal laboratory levels of illumination. For some experiments the flow tube was covered with a black shield to eliminate light, and no differences in the results were observed.

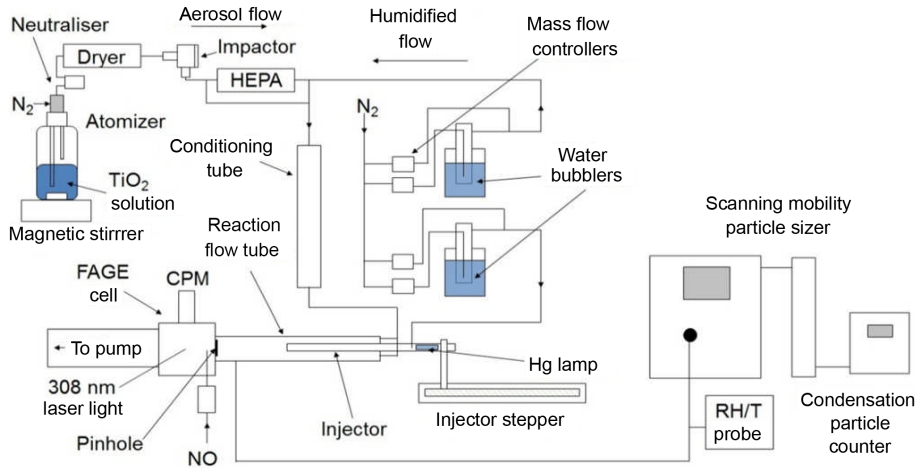

Figure 1. Schematic diagram of the aerosol flow tube experiment. CPM: channel photomultiplier; HEPA: high-efficiency particulate air filter; FAGE: fluorescence assay by gas expansion; RH/T: relative humidity/temperature.

Compressed nitrogen – which had been passed through a gas purification system (TSI 3074B) consisting of particle filters, a dryer and a carbon filter – was used as the carrier gas for the experiments. A humidified flow of TiO_2 particles was introduced through two inlets located at the rear of the aerosol flow tube, and the flow of HO_2 radicals enters the flow tube via the movable injector. The total flow through the flow tube (107 cm length, 5.9 cm ID) was 5.4 L min^{-1}, which resulted in a Reynolds number of 130 and therefore is considered laminar as confirmed by radial concentration gradient measurements of gases exiting the injector (George et al., 2013). Experiments consisted of moving the injector using a linear drive (BSL Engineering 15 KR4610A) to different fixed positions along the flow tube (30–70 cm from injector tip to HO_2 detector inlet in steps of 5 cm) corresponding to reaction times between $\sim$ 8 and 20 s from the injector, with detection of HO_2 at the end of the flow tube. All gas flows within the experiment were controlled using mass flow controllers (Brooks and MKS). The RH of the flow was measured using a probe (Rotronics) in the exhaust of the flow tube, which itself was calibrated against a dew point hygrometer (Buck Research Instruments CR-4).

2.2 Aerosol generation and detection

A solution of TiO_2 (Aldrich Chemistry 718467, 99.5 % Degussa, i.e. a blend of TiO_2 polymorphs 80 % anastase and 20 % rutile, 5 g in 500 mL of Milli-Q water) was placed in a commercial atomiser (TSI 3076) in order to produce a 1 L min^{-1} flow entrained with TiO_2 particles, referred to as the aerosol flow. The aerosol flow was then passed through a neutraliser (Grimm 5522) to reduce static wall losses, a diffusion drier (TSI 3062) and an impactor (TSI 1035900) to ensure that larger aerosols, beyond the detection range of the Scanning Mobility Particle Sizer (SMPS, $\sim$ 750 nm diameter), do not enter the aerosol flow tube. A high-efficiency particulate air (HEPA, PALL Life Sciences) filter situated within a bypass loop was used to control the number concentration of particles entering the aerosol flow tube. The aerosol flow was then mixed with a humidified flow of nitrogen (3 L min^{-1}) to control the RH within the system. The RH of the humidified flow was altered by changing the ratio of dry nitrogen and nitrogen passed through a water bubbler. This flow was then passed through a conditioning tube (residence time $\sim$ 6 s) before entering the aerosol flow tube to allow time for water adsorption onto the surface of the TiO_2 particles to equilibrate at the given RH.

The total surface area of TiO_2 particles available for heterogeneous reaction with HO_2 was measured with a SMPS instrument from the flow exiting the aerosol flow tube. Previous experiments showed that there is a negligible loss of aerosols during the transit of the flow tube (George et al., 2013). The SMPS consisted of a differential mobility analyser (DMA, TSI 3080, 3081) that creates a monodisperse flow of aerosols based on their electrical mobility, which is related to their size. A condensation particle counter (CPC, TSI 3775) connected in parallel to the DMA quantified particle number concentrations. These two instruments connected in parallel can be used to create an aerosol size distribution from which the total surface area and average radius of particles can be calculated by making the assumption that particles are spherical (as demonstrated experimentally in Sect. 3.2 below). The average diameter of the particles is 136 and 173 nm at RH = 11 and 37 % respectively.

2.3 HO_2 generation and detection

HO_2 radicals were produced within the movable injector (110 cm length, 1.9 cm OD, 1.6 cm ID) by passing a 1.3 L min^{-1} humidified flow of nitrogen (consisting of a mixture of 0.9 L min^{-1} of dry N_2 and 0.4 L min^{-1} N_2 passed through a water bubbler) containing trace amounts of oxygen

over a mercury lamp (L.O.T.-Oriel 6035) via the following reactions:

$$H_2O + h\nu(\lambda = 185\,\text{nm}) \rightarrow OH + H \quad \text{(R5)}$$

$$H + O_2 + M \rightarrow HO_2 + M. \quad \text{(R6)}$$

OH is also created by the photolysis of water vapour in Reaction (R5), but no OH was observed exiting the injector, presumably owing to rapid losses at the walls of the injector. HO_2 was sampled by a 0.7 mm diameter pinhole at the end of the flow tube, and after chemical conversion to OH by addition of excess NO (50 sccm, BOC, 99.5 %) just inside the pinhole, laser-induced fluorescence (LIF) at low-pressure (the fluorescence assay by gas expansion (FAGE) technique; Heard and Pilling, 2003) was used to measure OH. The relative LIF signal from converted HO_2 was calibrated using an established method (Winiberg et al., 2015) developed for field measurements of OH and HO_2 radicals. Hence the experiment is able to measure the absolute concentration of HO_2 during passage from the injector to the sampling inlet. The $Q_1(2)$ line of the OH ($A^2\Sigma^+ v' = 0 - X^2\Pi_i - v'' = 0$) transition at ~ 308 nm was used to detect OH. A Nd:YAG pumped dye laser (JDSU Q201-HD Q series, Sirah Cobra-Stretch) was used to produce the required 308 nm radiation (line width $\sim 0.1\,\text{cm}^{-1}$) at a pulse repetition rate of 5 kHz. As the flows through the movable injector ($1.3\,\text{L min}^{-1}$) and mercury lamp current (20 mA) were kept constant, it is assumed that the initial HO_2 concentration – $[HO_2]_0$ (defined in this investigation as $[HO_2]$ at the first injector position, i.e. 30 cm downstream of the injector), determined by calibration to be 1.6×10^9 molecule cm^{-3} – was the same for all experiments. These HO_2 concentrations are ~ 50 times higher than typical levels in the sunlit stratosphere (Wennberg et al., 1994). A reference fluorescence cell, in which a large concentration of OH was generated and detected by LIF, was used to facilitate the identification of OH lines and tune the laser wavelength. The FAGE cell was continuously evacuated using a combination of a rotary pump (Edwards, model E1M80) and a roots blower (EH1200), and was kept at 0.8–0.9 Torr, which was monitored using a capacitance monitor (Tylan General, CDC 11).

2.4 Experimental procedure and data analysis

The HO_2 signal was measured at eight positions as the moveable injector was drawn back from 30 to 70 cm using the linear stepper drive and again as the moveable injector was pushed forwards back to its initial position. The HO_2 signal was averaged over 20 s (average of twenty 1 s measurement points, each corresponding to 5000 laser shots) at each injector position with a 22 s delay between measurements at each injector position in order to allow time for mechanical vibrations to subside, and to ensure a full flush of the aerosol flow tube so that the LIF signal corresponds to HO_2 emitted from the injector position being measured. The laser power was recorded for each injector position and used to normalise the HO_2 signal to correct for any fluctuations in laser power (< 5 %). The HO_2 signals with the injector moving forwards and backwards were then averaged, and this procedure was repeated six times with varying concentrations of aerosols present in the aerosol flow tube. The wall loss rate of HO_2 (k_{wall}) was determined by recording the HO_2 decay in the absence of aerosols but at the same RH, and it was repeated four times for each experiment.

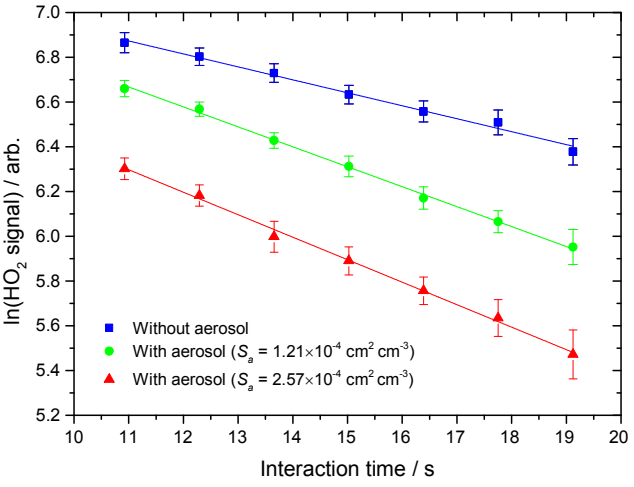

Figure 2. Measured HO_2 signal at different interaction times, in the presence of TiO_2 particles (surface area density: 1.21×10^{-4} and $2.57 \times 10^{-4}\,\text{cm}^2\,\text{cm}^{-3}$, green circles and red triangles respectively) and in their absence (blue squares). The RH in the aerosol flow tube was 11 %, the lowest used in this study. The lines represent linear least-squares fits to the data, yielding $k_{obs} = 0.079 \pm 0.005$ and $k_{obs} = 0.093 \pm 0.003\,\text{s}^{-1}$ (aerosols present, green circles and red triangles respectively) and $0.049 \pm 0.003\,\text{s}^{-1}$ (no aerosols, k_{wall}).

The HO_2 concentration as a function of time along the flow tube can be expressed as

$$\ln[HO_2]_t = \ln[HO_2]_0 - k_{obs}t, \quad (1)$$

where $[HO_2]_t$ and $[HO_2]_0$ are concentrations of HO_2 at time t and $t = 0$ respectively, and k_{obs} is the observed pseudo-first-order rate coefficient for HO_2 uptake. As the HO_2 signal is directly proportional to the concentration of HO_2, the gradient of a plot of ln(HO_2 signal) against time (calculated from the injector position and measured flow rate) yields k_{obs}, as shown in Fig. 2.

The flow tube was coated with halocarbon wax (Halocarbon Products Corporation, Halocarbon Wax Series 600) to reduce HO_2 wall loss rate (k_{wall}), and an average of k_{wall} from several determinations in the absence of aerosols was subtracted from k_{obs}. A correction (typically about 30 %) to account for non-plug flow conditions in the aerosol flow tube using the procedure outlined by Brown (1978) was applied to yield k', the pseudo-first-order loss of HO_2 by heterogeneous reaction with TiO_2 particles. The relationship between k' and

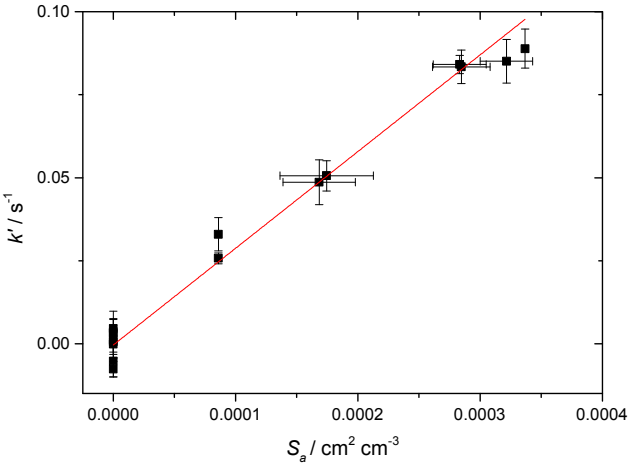

Figure 3. First-order rate coefficient for loss of HO_2 due to heterogeneous reaction with TiO_2 particles at different total surface areas for $T = 296$ K and RH = 37 %. The gradient yielded a value of $\gamma(HO_2) = (2.68 \pm 0.01) \times 10^{-2}$, with the uncertainty representing 2σ random errors from the fit (95 % confidence limits).

total surface area of TiO_2 particles (S_a) can be expressed as (George et al., 2013)

$$k' = \frac{w_{HO_2} \gamma_{obs} S_a}{4}, \quad (2)$$

where w_{HO_2} is the mean velocity of HO_2 ($\sim 435\,ms^{-1}$ at 293 K) and γ_{obs} is the observed reactive uptake coefficient, obtained from a plot of k' versus S_a, an example of which is given in Fig. 3. γ_{obs} was in turn corrected (typically ~ 1 %) to account for the gas diffusion limitation (Fuchs and Sutugin, 1970), to yield $\gamma(HO_2)$.

2.5 TOMCAT model description

The TOMCAT offline 3-D CTM (Chipperfield, 1999, 2006) has been used to predict the impact of the heterogeneous reaction of TiO_2 with HO_2 to stratospheric concentrations of O_3 and HO_2. The model has been widely used in previous studies of stratospheric chemistry and performs well in reproducing stratospheric ozone and the trace species which control its distribution (Chipperfield et al., 2015). The model includes a detailed treatment of stratospheric chemistry of O_x, HO_x, NO_y, Cl_y and Br_y species along with the main source gases. The model has a comprehensive gas-phase chemistry scheme and includes a number of heterogeneous reactions on stratospheric sulfate aerosols and polar stratospheric clouds (Chipperfield, 1999).

The loss rate of HO_2 due to heterogeneous reaction with TiO_2 was included in the model as

$$k = 0.25 S_a w_{HO_2} \gamma\,(HO_2)\,, \quad (3)$$

where S_a is the surface area density of TiO_2, and w_{HO_2} and $\gamma(HO_2)$ are defined above. Three TOMCAT simulations were performed at a horizontal resolution of 5.6° × 5.6° and 32 levels from the surface to ~ 60 km. The model was forced with wind and temperature fields from the European Centre for Medium-Range Weather Forecasts (ECMWF) ERA-Interim reanalyses and integrated for 2 years from January 2007 until December 2008, initialised with the output from a standard TOMCAT run which had spun up from 1977. More information on the model experiments is given in Sect. 3.3.

Table 1. Reactive HO_2 uptake coefficients, $\gamma(HO_2)$, for TiO_2 particles at different RH.

RH (%) ± 1.0	$\gamma(HO_2)/10^{-2}$
11.1	2.08 ± 0.11
11.8	2.11 ± 0.13
24.9	2.48 ± 0.33
29.1	2.54 ± 0.18
37.5	2.68 ± 0.09
45.1	2.90 ± 0.53
45.3	2.92 ± 0.37
63.1	3.43 ± 0.27
66.4	3.65 ± 0.70

3 Results and discussion

3.1 The reactive uptake coefficient dependence with relative humidity

The reactive uptake coefficient for HO_2 radicals, $\gamma(HO_2)$, onto TiO_2 particles was determined at eight different RHs (11–66%), as shown in Fig. 4 and summarised in Table 1. The number of monolayers of water adsorbed onto the surface of TiO_2 particles has been previously determined experimentally by transmission Fourier transform infrared (FTIR) spectroscopy (Goodman et al., 2001) and is also shown as a function of RH in Fig. 4.

The results clearly show a positive dependence of $\gamma(HO_2)$ across the range of RH investigated; as shown in Fig. 5, $\gamma(HO_2)$ correlates well with the number of monolayers of water adsorbed onto the TiO_2 particles, V/V_m, which was determined by Goodman et al. (2001) and parameterised by Eq. (4):

$$\frac{V}{V_m} = \left[\frac{c\left(\frac{P}{P_0}\right)}{1-\left(\frac{P}{P_0}\right)}\right]\left[\frac{1-(n+1)\left(\frac{P}{P_0}\right)^n + n\left(\frac{P}{P_0}\right)^{n+1}}{1+(c-1)\left(\frac{P}{P_0}\right) - c\left(\frac{P}{P_0}\right)^{n+1}}\right], \quad (4)$$

where V is the volume of gas (water vapour) adsorbed at equilibrium pressure P, V_m is volume of gas necessary to cover the surface of the adsorbent TiO_2 particles with a complete monolayer, P is the equilibrium pressure of the adsorbing gas, P_0 is the saturation vapour pressure of the adsorbing gas at that temperature, c is a temperature-dependent

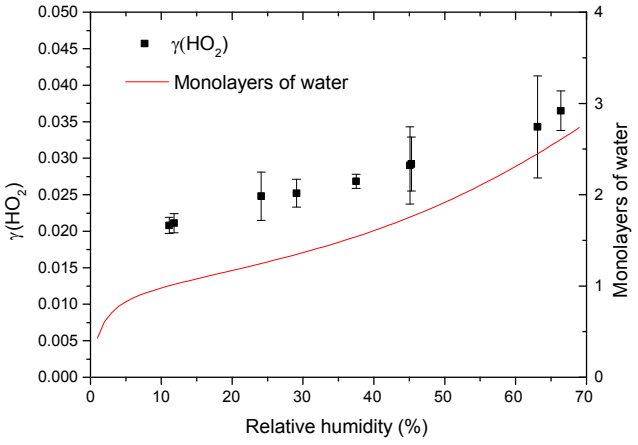

Figure 4. Reactive uptake coefficients of HO_2, $\gamma(HO_2)$, onto airborne TiO_2 particles (black squares, left y axis) at different RH for $T = 295 \pm 2$ K. The number of monolayers of the adsorbed water on TiO_2 particles (red curve, right y axis) at 296 K is also plotted as a function of RH, determined using FTIR spectroscopy (Goodman et al., 2001).

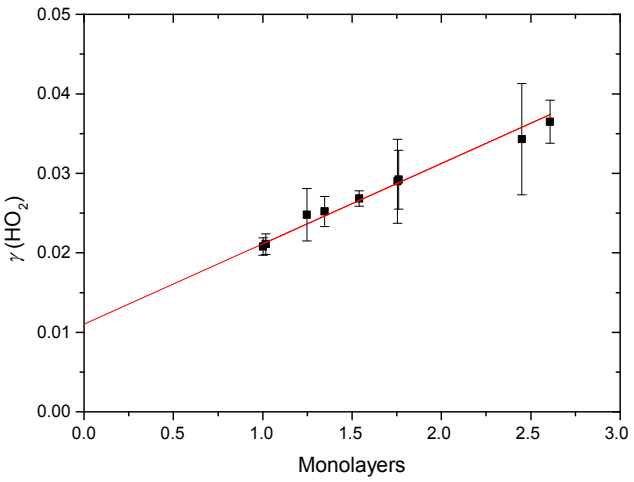

Figure 5. Variation of the reactive uptake coefficient, $\gamma(HO_2)$, with the number of monolayers of water surrounding TiO_2 particles (as determined by Goodman et al., 2001) for $T = 295 \pm 2$ K. The red line represents a linear least-squares fit to the data ($r^2 = 0.987$).

constant related to the enthalpies of adsorption of the first and higher layers, and n is the asymptotic limit of monolayers (~ 8).

Wall losses of HO_2 also increase as RH is increased within the aerosol flow tube; so in the absence of aerosols, the $[HO_2]$ for a given distance from the injector will decrease with RH. Previous work in this laboratory has shown that $\gamma(HO_2)$ for uptake on ATD aerosols increases as the $[HO_2]$ is lowered (Matthews et al., 2014), and hence some of the positive dependence of $\gamma(HO_2)$ with RH shown in Fig. 4 might be expected simply owing to the $[HO_2]$ impinging on the aerosol for a given injector position decreasing with RH. To investigate this further, uptake onto TiO_2 at RH = 11 % was measured as a function of $[HO_2]_0$ exiting the injector, and $\gamma(HO_2)$ increased from 2.08×10^{-2} to 2.72×10^{-2} as $[HO_2]_0$ was decreased from 1.6×10^9 to 8.9×10^8 molecule cm^{-3}. However, the wall loss rate for HO_2 only increased from 0.049 to 0.079 s^{-1} across the entire range of RH (11 to 66 %), resulting in only a small change in $[HO_2]$: decreases of $\sim 2.6 \times 10^8$ and $\sim 2.7 \times 10^8$ molecule cm^{-3} at the first and last injector position respectively. In previous studies of HO_2 uptake onto ATD (Matthews et al., 2014) it was shown that the increase of $\gamma(HO_2)$ with decreasing $[HO_2]$ is linear. Therefore, when assuming the same behaviour for uptake onto TiO_2 particles, the expected change in $\gamma(HO_2)$ as a result of RH increasing from 11 to 66 % due only to a change in initial HO_2 concentration is only $\Delta\gamma(HO_2) = 0.0023$ (or ~ 6 % of the averaged measured $\gamma(HO_2)$ across this range). Hence the 75 % increase in $\gamma(HO_2)$ observed in Fig. 4 across this range of RH has a different cause.

Figure 5 shows that, for the range of RH studied, $\gamma(HO_2)$ is a linear function of the number of monolayers of water surrounding a TiO_2 particle, suggesting that water plays a role in the reactive HO_2 uptake process on TiO_2 particles. Studies using ambient pressure photoelectron spectroscopy (APPES) (Yamamoto et al., 2008) have shown that water adsorption on rutile, a polymorph of TiO_2 (110), occurs in distinct steps, as illustrated in Fig. 6.

First, water molecules dissociate at O vacancies (V_{bridge}) at bridge sites, producing a stoichiometric amount of adjacent bridging OH groups (OH_{bridge}) equal to twice the initial vacancy concentration upon initial exposure of rutile to water vapour (see Fig. 6):

$$H_2O + V_{bridge} + O_{bridge} = 2OH_{bridge}. \quad \text{(R7)}$$

This step takes place even at very low RH, with these bridging OH groups acting as nucleation sites for subsequent water adsorption by anchoring water molecules to form strongly bound OH–H_2O complexes. The OH–H_2O complexes continue to act as nucleation centres for further water adsorption. The wetting properties of TiO_2 (110) are thus driven by moderate amounts of strongly attractive OH sites that nucleate water molecules. These OH–H_2O complexes have a relatively high enthalpy of adsorption for water of -72 kJ mol^{-1} (Ketteler et al., 2007), whereas additional adsorption of water beyond a monolayer of water coverage is more characterised by enthalpies associated with the bulk enthalpy of water condensation (-45 kJ mol^{-1}) (Chen et al., 2012), explaining the variation of the number of monolayers of water with RH shown in Fig. 4. Computational studies (Aloisio and Francisco, 1998) showed that in the gas phase HO_2 can also readily form complexes with water through hydrogen bonding with a binding energy of 28.9 kJ mol^{-1}. The observed correlation of $\gamma(HO_2)$ with the number of monolayers of water surrounding TiO_2 particles could be explained

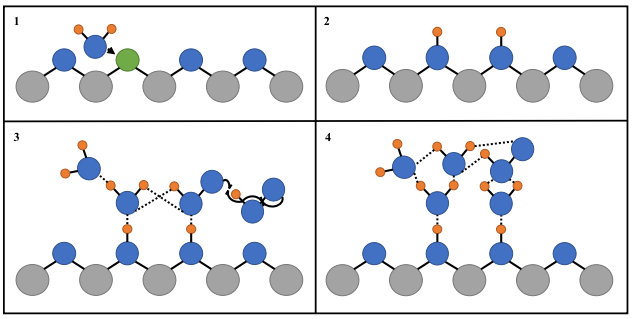

Figure 6. Simplified diagram of the important steps of HO_2 reactive uptake onto the surface of TiO_2. Grey circles: Ti; blue circles: O; orange circles: H; green circles: oxygen vacancy (V_{bridge}): solid black lines: chemical bond; and dashed lines: hydrogen bond. **(1)** Diffusion of water molecule towards a bridging O vacancy. **(2)** Resultant formation of two neighbouring bridging OH groups at the original site of the O vacancy. **(3)** Bridging OH groups acting as anchoring sites for water and HO_2 adsorption via hydrogen bonding, leading to multilayer water adsorption and HO_2 self-reaction via an Eley–Rideal type mechanism. **(4)** The build-up of a more extensive hydrogen bonded network as more water molecules adsorb onto the particle, which stabilises HO_2 increasing its desorption lifetime and hence probability that it will react.

by two effects: (1) an increase in the network of hydrogen bonding would increase the stability of a molecular system, $\sim 20.9\,kJ\,mol^{-1}$, for each hydrogen bond (Joshi and Ghanty, 2013), or (2) simply more HO_2 can adsorb onto the particle surface as the number of available sites for hydrogen bonding increases. An increase in the adsorption lifetime of HO_2 owing to the more extended H-bonding network (Joshi and Ghanty, 2013) will result in an increased probability of HO_2 reacting with another HO_2, increasing the value of $\gamma(HO_2)$:

$$HO_2 + HO_2 \rightarrow H_2O_2 + O_2. \quad \text{(R8)}$$

For up to ~ 2 monolayers of H_2O, an Eley–Rideal (ER) mechanism of a gas-phase HO_2 molecule reacting with an adsorbed HO_2 is more likely than for two adsorbed HO_2 molecules diffusing together to react via a Langmuir–Hinshelwood (LH) mechanism. The coverage of V_{bridge} across the surface of TiO_2 (110) is 0.125 monolayers (i.e. one vacancy for every eight unit cells) (Ketteler et al., 2007), meaning water will initially adsorb onto the surface of the particle in clusters. As the binding energy of the HO_2 water complex is fairly high, the rate of HO_2 diffusion across the surface after the initial adsorption at a bridging site will be slow, making a LH type mechanism seem unlikely. Above ~ 2 monolayers, the adsorbed water clusters will begin to interact with each other via an extended H-bonded network more characteristic of bulk liquid water, allowing HO_2 to diffuse around the thin surface film of water with thermodynamic properties similar to liquid water (Ketteler et al., 2007).

The superoxide ion, O_2^-, which is the conjugate base of HO_2, reacts with HO_2 over 100 times quicker than with HO_2 via

$$HO_2 + O_2^- + H_2O \rightarrow H_2O_2 + O_2 + OH^-. \quad \text{(R9)}$$

It is unlikely that O_2^- will form readily on the surface of the particle at low coverages of water. O_2^- can form on surfaces via direct surface–oxygen electron transfer, photo-induced electron transfer, surface intermolecular electron transfer or decomposition of hydrogen peroxide (H_2O_2) (Anpo et al., 1999). The dissociation of HO_2 to O_2^- occurs in bulk liquid ($pK_a = 4.7$; Thornton and Abbatt, 2005); however, water surrounding the particles only begins to acquire liquid-like properties once the coverage of water is greater than ~ 2 monolayers. If significant formation of O_2^- does occur above ~ 2 monolayers of H_2O, then, owing to its much higher reactivity, some deviation from linearity of $\gamma(HO_2)$ versus monolayers of water (Fig. 5) might be expected. However, this was not observed, although the number of data points is very limited.

3.2 Comparison of $\gamma(HO_2)$ with literature values

There are previous studies of HO_2 uptake onto ATD (Matthews et al., 2014), a proxy for mineral dust, and both N_2O_5 (Tang et al., 2014) and $ClONO_2$ (Tang et al., 2016) uptake onto TiO_2 particles. Values of $\gamma(HO_2)$ measured for ATD are comparable to those measured onto TiO_2 particles at similar concentrations of HO_2 in the aerosol flow tube ($\gamma(HO_2)_{ATD} \sim 0.008$–$0.030$). For ATD, $\gamma(HO_2)$ was only determined at four values of RH, but a general increase with RH was observed (although there was a dip around RH = 50 % before a further increase), consistent with HO_2 uptake being driven by the number of defects in the crystal lattice of mineral dust surfaces, which provides bridging OH groups upon exposure to water and subsequently by the number of monolayers of water adsorbed onto the surface of such aerosols. The number of monolayers of water on the ATD surface at different RH has been determined (Gustafsson et al., 2005) and also showed a general increase with RH but with a shoulder around RH = 50 %, where the observed $\gamma(HO_2)$ also contained a small dip.

Values of $\gamma(N_2O_5)$ (Tang et al., 2014) and $\gamma(ClONO_2)$ (Tang et al., 2016) for uptake onto TiO_2 particles were an order of magnitude lower than $\gamma(HO_2)$ and may be associated with the lower polarity of these molecules than that of HO_2. It is likely that, as with uptake of HO_2, both N_2O_5 and $ClONO_2$ react with TiO_2 via complexing with bridging OH groups and adsorbed H_2O; therefore less polar molecules will be less bound to the surface and more likely to desorb back into the gas phase, leading to a smaller γ. The dependence upon RH for $\gamma(N_2O_5)$ onto TiO_2 is also different to that for HO_2 observed here, with a small decrease of $\gamma(N_2O_5)$ observed as the RH is increased from ~ 5 to 23 %, where a minimum is reached; then beyond 23 %, $\gamma(N_2O_5)$

increases as RH is increased (Tang et al., 2014). Competition between water and N_2O_5 for surface active OH groups was suggested for the initial observed decrease in $\gamma(N_2O_5)$ with RH, whereas for RH $> \sim 23$ % heterogeneous hydrolysis of N_2O_5 to form HNO_3 starts to drive reactive uptake, resulting in an increase of $\gamma(N_2O_5)$ (Tang et al., 2014). Measurements of $\gamma(ClONO_2)$ onto TiO_2 particles were only made at two values of RH, insufficient to determine any systematic dependence, although Tang et al. (2016) expected $\gamma(ClONO_2)$ to increase as more water adsorbs onto the surface of TiO_2 particles.

Measurements of $\gamma(HO_2)$ have been made onto sulfuric acid aerosols and thin films. These values are not consistent and range from > 0.1 to < 0.01 (Cooper and Abbatt, 1996; Thornton and Abbatt, 2005; Hanson et al., 1992; Gershenzon et al., 1995). The most recent measurement of $\gamma(HO_2)$ on aqueous-phase sulfuric acid aerosols was conducted at 35 % RH (Thornton and Abbatt, 2005). That study estimated a value of $\gamma(HO_2) = 0.006 \pm 0.004$, lower than onto TiO_2 aerosols. Whilst the aerosols in that study are unlike sulfuric acid aerosols in the stratosphere, formed via condensation of sulfuric acid vapour onto existing solid aerosols, the relatively low value of $\gamma(HO_2)$ measured is consistent with the likely low partitioning of HO_2 to its more reactive conjugate base, O_2^-, and a lower solubility of HO_2 in aerosols with a low pH. The study concludes that heterogeneous uptake of HO_2 onto sulfuric acid aerosols would show a strong negative temperature dependence driven by the temperature dependence of the Henry's Law coefficient. It is likely that at temperatures typical of the lower stratosphere (205–215 K) $\gamma(HO_2)$ for uptake onto sulfuric acid particles approach 1 (Gershenzon et al., 1995).

George et al. (2013) previously measured $\gamma(HO_2)$ onto dry salt aerosols. Values of $\gamma(HO_2)$ for NaCl and $(NH_4)_2SO_4$ at RH values (33–54 %) below their deliquescence point were below the limit of detection ($\gamma(HO_2) < 0.004$). Values of $\gamma(HO_2)$ for TiO_2 reported here (Fig. 4 and Table 1) are more than an order of magnitude greater than that of solid salts, even for RH = 11 %. A possible explanation for the difference in $\gamma(HO_2)$ values could be that, even though the sizes of the aerosols determined by the SMPS are similar, dry salt aerosols are more spherical in shape than TiO_2 particles, which may be more fractal in nature. As the SMPS indirectly measures the surface area of aerosols by measuring their mobility through an electric field, an assumption that the aerosol is spherical has to be made. If this is not the case, this may lead to a significant under-prediction of the surface area of non-spherical aerosols and therefore an over-prediction of $\gamma(HO_2)$. In order to measure the geometry of the TiO_2 particles, a scanning electron microscope (SEM, FEI Nova NanoSEM 450) operating at 3 kV was used to image the TiO_2 nanoparticles used within these experiments. Samples for the SEM were prepared by dispersing the nanoparticles in ethanol and allowing a drop of this solution to dry on a silicon wafer. The wafer with nanoparticles was then mounted on SEM stubs using conductive carbon tapes and coated with 2 nm of Ir, using a Cressington 208HR high-resolution sputter coater. Figure 7 shows an example of an SEM image providing evidence that the TiO_2 particles are spherical and therefore that any error associated with SMPS measurements of surface area is minimal. A more likely explanation for the higher $\gamma(HO_2)$ for TiO_2 particles is that dry salt aerosols do not adsorb a significant amount of water onto their surface until the deliquescence point is reached, whereas at RH = 11 % Fig. 4 shows that the TiO_2 particles already have a monolayer coverage which can form relatively strongly bound complexes with HO_2. Measurements of $\gamma(HO_2)$ for uptake onto aqueous salt aerosols show that $\gamma(HO_2)$ significantly increases above the deliquescence point (George et al., 2013) and is comparable to $\gamma(HO_2)$ measured for TiO_2 ($\gamma(HO_2) \sim 0.01$).

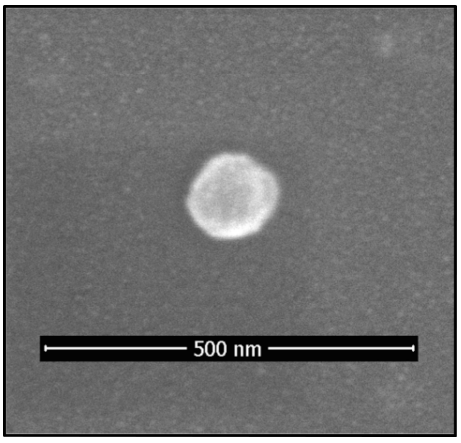

Figure 7. SEM image of a single TiO_2 particle magnified 80 000 × used within this study.

3.3 Implications of HO_2 uptake by TiO_2 for stratospheric chemistry

The effect of HO_2 uptake onto TiO_2 particles upon the stratospheric concentrations of HO_2 and O_3 was assessed using the TOMCAT model (Chipperfield, 1999, 2006). At RH relevant to the lower stratosphere (<40%) the measurements showed that $\gamma(HO_2)$ is in the range 0.020–0.028 at 295 K. An inverse temperature dependence of $\gamma(HO_2)$ onto dry seasalt aerosols has previously been observed (Remorov et al., 2002); although there have been no systematic experimental studies of the temperature dependence of $\gamma(HO_2)$, parameterisations have developed (Thornton et al., 2008; Macintyre and Evans, 2011). At stratospherically relevant temperatures (T = 200–220 K), $\gamma(HO_2)$ is likely to be considerably larger than observed at 295 K; however it is not possible to cool the aerosol flow tube/SMPS system to verify this experimentally. Therefore $\gamma(HO_2) = 1$ was used in the model simulations representing an upper limit, with three TOMCAT simulations performed as follows. A control simulation, sim-

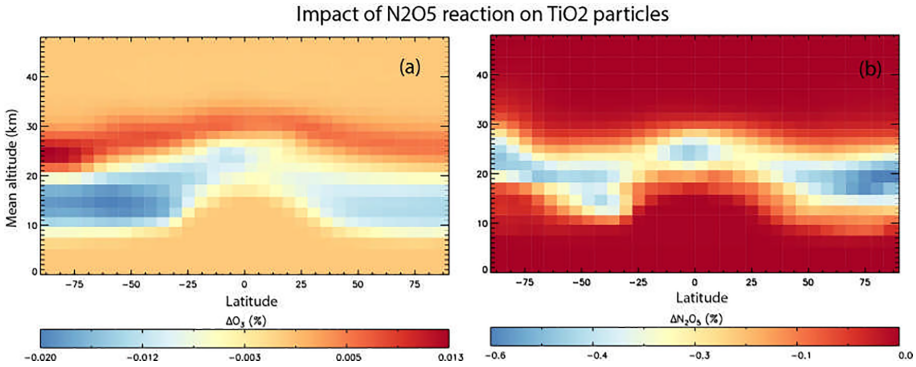

Figure 8. Annual mean change (%) in atmospheric O_3 **(a)** and N_2O_5 **(b)** calculated using the TOMCAT 3-D model from inclusion of heterogeneous loss of N_2O_5 on TiO_2 particles for 2008 and using $\gamma(N_2O_5) = 0.005$.

ilar to that presented in Chipperfield et al. (2015), did not include TiO_2 particles. A specified latitude–height distribution of TiO_2 particles was then included in two simulations with an effective aerosol surface area density equal to that of sulfate aerosols in 1992, the year after the eruption of Mt Pinatubo. This is an assumption which allows for the fact that less TiO_2 mass is needed in order to produce the same radiative impact as sulfate aerosol from Mt Pinatubo, but the TiO_2 particle size is smaller. Hence these effects largely cancel (Tang et al., 2014). Stratospheric injection via a geoengineering solution will result initially in a different distribution of TiO_2 particles compared with after the Mt Pinatubo eruption, but it is assumed that following mixing and transport the distributions would resemble one another and not lead to any significant difference in model behaviour and the conclusions drawn. Support from this assumption comes from a model run in which a globally uniform distribution of TiO_2 was assumed initially and which yielded very similar results for the impact of $\gamma(HO_2)$.

The first of these simulations included only the loss of N_2O_5 on TiO_2 particles with $\gamma(N_2O_5) = 0.005$, the upper limit used in the modelling of Tang et al. (2014), which allows us to compare our results with their study. The second TiO_2 simulation also included the loss of HO_2 on TiO_2 particles with a $\gamma(HO_2) = 1$, as discussed above. Figure 8 shows the impact of including heterogeneous loss of N_2O_5 on TiO_2 particles in the model.

N_2O_5 is decreased by up to 0.5 % in the region of TiO_2 particles, which is assumed to follow the distribution of sulfate particles after the Mt Pinatubo eruption, in order to follow the approach of previous modelling studies. Assuming a globally uniform distribution initially yielded results that were very similar. Inclusion of uptake is only a minor effect and considerably smaller than the impact of around −20 % modelled by Tang et al. (2004) for the same assumed $\gamma(N_2O_5) = 0.005$. The reasons for this are not clear, although it is noted that the effect modelled in our offline chemical transport model, with specified meteorology, is clearly confined to regions of high aerosol loading. The impacts modelled in the nudged chemistry–climate model study of Tang et al. (2004) are not confined to the region of high aerosol and even extend to the upper stratosphere. It is possible that their simulations, although nudged, also include some dynamical feedback which enhances an otherwise small signal. Figure 8 also shows that the resulting impact on O_3 is small with changes less than 0.02 %. The model produces a region of slight decrease in the very low stratosphere, with a region of slight increase above.

Figure 9 shows results from the simulation which also included the loss of HO_2 on stratospheric TiO_2 particles, and using $\gamma(HO_2) = 1$. It is evident that HO_2 loss due to heterogeneous reaction between HO_2 and TiO_2 particles in 2008 is < 1 % and is confined to the lower stratosphere, where it is assumed TiO_2 particles are located. Figure 9 also shows that the subsequent effect of the TiO_2 particles on the O_3 concentrations through the effects of this reaction is also small (< 0.1 %), with a small decrease in the tropical upper troposphere/lower stratosphere and a small increase at all latitudes in the lower stratosphere. This small effect of TiO_2 particles on stratospheric HO_2 and O_3 concentrations is due to the reactive nature and short lifetime of HO_2. The species readily reacts with other gas-phase species (e.g. O_3), and so loss on TiO_2 surfaces does not compete significantly.

4 Conclusions and further work

The reactive uptake coefficients for the heterogeneous reaction of HO_2 onto TiO_2 particles were measured at different RH and at room temperature for the first time using an aerosol flow tube reactor coupled with a sensitive FAGE HO_2 detection system. A range of HO_2 uptake coefficients on TiO_2 particles were measured varying from $\gamma(HO_2) = 0.021 \pm 0.001$ to 0.036 ± 0.007 for RH over the range 11 to 66 % respectively. The HO_2 uptake coefficient showed a positive dependence on RH which correlated well with the number of monolayers of water adsorbed onto the TiO_2 particle. These results suggest a mechanism by which

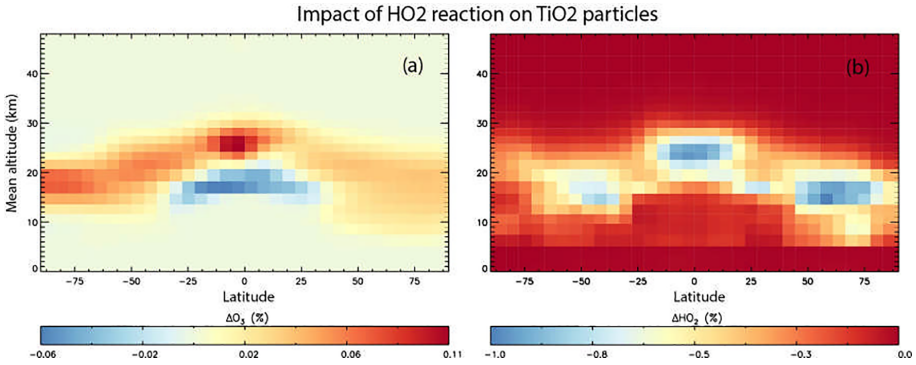

Figure 9. Annual mean change (%) in atmospheric O_3 **(a)** and HO_2 **(b)** calculated using the TOMCAT 3-D model from inclusion of heterogeneous loss of HO_2 on TiO_2 particles for 2008, and using $\gamma(HO_2) = 1$.

HO_2 adsorbs to the surface of the TiO_2 particle by forming complexes with water molecules bound to bridging OH groups. As the number of water layers increases, so does the network of hydrogen bonds that stabilises HO_2, leading to a longer adsorption lifetime and increased $\gamma(HO_2)$. The TOMCAT chemical transport model was used to evaluate the possible effects of HO_2 uptake (using an upper limit of $\gamma(HO_2) = 1$) onto the surface of TiO_2 particles on the stratospheric concentrations of HO_2 and O_3. The amount of TiO_2 used was chosen to achieve a similar cooling to that following the Mt Pinatubo eruption, but the model predicted a very small loss of both stratospheric HO_2 and O_3. TiO_2 possesses photocatalytic properties, and water adsorbed onto its surface may dissociate under stratospheric illumination, providing a source of radicals (Chen et al., 2012; Romanias et al., 2012). Production of OH and HO_2 from irradiated TiO_2 surfaces should be evaluated in future studies together with studies of uptake at lower temperature to fully understand the consequences of injection of TiO_2 particles into the stratosphere.

Data availability. Data from the experiments and TOMCAT model simulations can be obtained by contacting Dwayne Heard (d.e.heard@leeds.ac.uk) and Martyn Chipperfield (m.chipperfield@leeds.ac.uk), respectively.

Competing interests. The authors declare that they have no conflict of interest.

Acknowledgements. We are grateful to the Natural Environment Research Council for funding a studentship (Daniel R. Moon) and for funding the aerosol flow tube apparatus (grant number NE/F020651/1). Trevor Ingham, Paul W. Seakins and Dwayne E. Heard are also grateful to the NERC-funded National Centre for Atmospheric Science for ongoing support. The TOMCAT modelling work was supported by the EU StratoClim project (FP7 grant 603557). We thank Wuhu Feng (NCAS Leeds) for help with the model. The model simulations were performed on the University of Leeds and N8 HPC system.

Edited by: Allan Bertram
Reviewed by: two anonymous referees

References

Aloisio, S. and Francisco, J. S.: Existence of a hydroperoxy and water (HO_2 center dot H_2O) radical complex, J. Phys. Chem. A, 102, 1899–1902, https://doi.org/10.1021/jp972173p, 1998.

Ammann, M., Cox, R. A., Crowley, J. N., Jenkin, M. E., Mellouki, A., Rossi, M. J., Troe, J., and Wallington, T. J.: Evaluated kinetic and photochemical data for atmospheric chemistry: Volume VI – heterogeneous reactions with liquid substrates, Atmos. Chem. Phys., 13, 8045–8228, https://doi.org/10.5194/acp-13-8045-2013, 2013.

Anpo, M., Che, M., Fubini, B., Garrone, E., Giamello, E., and Paganini, M. C.: Generation of superoxide ions at oxide surfaces, Top. Catalys., 8, 189–198, https://doi.org/10.1023/a:1019117328935, 1999.

Bedjanian, Y., Romanias, M. N., and El Zein, A.: Uptake of HO_2 radicals on Arizona Test Dust, Atmos. Chem. Phys., 13, 6461–6471, https://doi.org/10.5194/acp-13-6461-2013, 2013.

Brown, R. L.: Tubular flow reactors with 1st-order kinetics, J. Res. Natl. Bureau Stand., 83, 1–8, 1978.

Chen, H., Nanayakkara, C. E., and Grassian, V. H.: Titanium Dioxide Photocatalysis in Atmospheric Chemistry, Chem. Rev., 112, 5919–5948, https://doi.org/10.1021/cr3002092, 2012.

Chipperfield, M. P.: Multiannual simulations with a three-dimensional chemical transport model, J. Geophys. Res.-Atmos., 104, 1781–1805, https://doi.org/10.1029/98jd02597, 1999.

Chipperfield, M. P.: New version of the TOMCAT/SLIMCAT off-line chemical transport model: Intercomparison of stratospheric tracer experiments, Q. J. Roy. Meteorol. Soc., 132, 1179–1203, https://doi.org/10.1256/qj.05.51, 2006.

Chipperfield, M. P., Dhomse, S. S., Feng, W., McKenzie, R. L., Velders, G. J. M., and Pyle, J. A.: Quantifying the ozone and ultraviolet benefits already achieved by the Montreal Protocol, Nat. Commun., 6, 8, https://doi.org/10.1038/ncomms8233, 2015.

Cooper, P. L. and Abbatt, J. P. D.: Heterogeneous interactions of OH and HO_2 radicals with surfaces characteristic of atmospheric particulate matter, J. Phys. Chem., 100, 2249–2254, 1996.

Dutton, E. G. and Christy, J. R.: Solar radiative forcing at selected locations and evidence for global lower tropospheric cooling following the eruptions of El-Chichon and Pinatubo, Geophys. Res. Lett., 19, 2313–2316, https://doi.org/10.1029/92gl02495, 1992.

Fuchs, N. A. and Sutugin, A. G.: Highly dispersed aerosols, Ann Arbor Science, London, 1970.

George, I. J., Matthews, P. S., Whalley, L. K., Brooks, B., Goddard, A., Baeza-Romero, M. T., and Heard, D. E.: Measurements of uptake coefficients for heterogeneous loss of HO_2 onto submicron inorganic salt aerosols, Phys. Chem. Chem. Phys., 15, 12829–12845, https://doi.org/10.1039/c3cp51831k, 2013.

Gershenzon, Y. M., Grigorieva, V. M., Ivanov, A. V., and Remorov, R. G.: O_3 and OH sensitivity to heterogeneous sinks of HO_x and CH_3O_2 on aerosol particles, Faraday Discuss., 100, 83–100, 1995.

Goodman, A. L., Bernard, E. T., and Grassian, V. H.: Spectroscopic study of nitric acid and water adsorption on oxide particles: Enhanced nitric acid uptake kinetics in the presence of adsorbed water, J. Phys. Chem. A, 105, 6443–6457, https://doi.org/10.1021/jp003722l, 2001.

Gustafsson, R. J., Orlov, A., Badger, C. L., Griffiths, P. T., Cox, R. A., and Lambert, R. M.: A comprehensive evaluation of water uptake on atmospherically relevant mineral surfaces: DRIFT spectroscopy, thermogravimetric analysis and aerosol growth measurements, Atmos. Chem. Phys., 5, 3415–3421, https://doi.org/10.5194/acp-5-3415-2005, 2005.

Hanson, D. R., Burkholder, J. B., Howard, C. J., and Ravishankara, A. R.: Measurement of hydroxyl and hydroperoxy radical uptake coefficients on water and sulfuric acid surfaces, J. Phys. Chem., 96, 4979–4985, https://doi.org/10.1021/j100191a046, 1992.

Heard, D. E. and Pilling, M. J.: Measurement of OH and HO_2 in the troposphere, Chem. Rev., 103, 5163–5198, 2003.

Holloway, A. M. and Wayne, R. P.: Atmospheric Chemistry, RSC Publishing, Cambridge, UK, 2010.

Huneeus, N., Schulz, M., Balkanski, Y., Griesfeller, J., Prospero, J., Kinne, S., Bauer, S., Boucher, O., Chin, M., Dentener, F., Diehl, T., Easter, R., Fillmore, D., Ghan, S., Ginoux, P., Grini, A., Horowitz, L., Koch, D., Krol, M. C., Landing, W., Liu, X., Mahowald, N., Miller, R., Morcrette, J. J., Myhre, G., Penner, J., Perlwitz, J., Stier, P., Takemura, T., and Zender, C. S.: Global dust model intercomparison in AeroCom phase I, Atmos. Chem. Phys., 11, 7781–7816, https://doi.org/10.5194/acp-11-7781-2011, 2011.

Joshi, R. and Ghanty, T. K.: Hydrogen bonding interaction between HO_2 radical and selected organic acids, RCOOH ($R = CH_3$, H, Cl and F), Chem. Phys. Lett., 584, 43–48, https://doi.org/10.1016/j.cplett.2013.08.025, 2013.

Karagulian, F., Santschi, C., and Rossi, M. J.: The heterogeneous chemical kinetics of N_2O_5 on $CaCO_3$ and other atmospheric mineral dust surrogates, Atmos. Chem. Phys., 6, 1373–1388, https://doi.org/10.5194/acp-6-1373-2006, 2006.

Ketteler, G., Yamamoto, S., Bluhm, H., Andersson, K., Starr, D. E., Ogletree, D. F., Ogasawara, H., Nilsson, A., and Salmeron, M.: The nature of water nucleation sites on TiO_2(110) surfaces revealed by ambient pressure X-ray photoelectron spectroscopy, J. Phys. Chem. C, 111, 8278–8282, https://doi.org/10.1021/jp068606i, 2007.

Lakey, P. S. J., George, I. J., Baeza-Romero, M. T., Whalley, L. K., and Heard, D. E.: Organics Substantially Reduce HO2 Uptake onto Aerosols Containing Transition Metal ions, J. Phys. Chem. A, 120, 1421–1430, https://doi.org/10.1021/acs.jpca.5b06316, 2016.

Macintyre, H. L. and Evans, M. J.: Parameterisation and impact of aerosol uptake of HO_2 on a global tropospheric model, Atmos. Chem. Phys., 11, 10965–10974, https://doi.org/10.5194/acp-11-10965-2011, 2011.

Matthews, P. S. J., Baeza-Romero, M. T., Whalley, L. K., and Heard, D. E.: Uptake of HO_2 radicals onto Arizona test dust particles using an aerosol flow tube, Atmos. Chem. Phys., 14, 7397–7408, https://doi.org/10.5194/acp-14-7397-2014, 2014.

McCormick, M. P. and Veiga, R. E.: SAGE II measurements of early Pinatubo aerosols, Geophys. Res. Lett., 2, 155–158, 1992.

McCormick, M. P., Thomason, L. W., and Trepte, C. R.: Atmospheric effects of the Mt. Pinatubo eruption, Nature, 373, 399–404, https://doi.org/10.1038/373399a0, 1995.

Pope, F. D., Braesicke, P., Grainger, R. G., Kalberer, M., Watson, I. M., Davidson, P. J., and Cox, R. A.: Stratospheric aerosol particles and solar-radiation management, Nat. Clim. Change, 2, 713–719, https://doi.org/10.1038/nclimate1528, 2012.

Remorov, R. G., Gershenzon, Y. M., Molina, L. T., and Molina, M. J.: Kinetics and mechanism of HO_2 uptake on solid NaCl, J. Phys. Chem. A, 106, 4558–4565, https://doi.org/10.1021/jp013179o, 2002.

Romanias, M. N., El Zein, A., and Bedjanian, Y.: Heterogeneous Interaction of H_2O_2 with TiO_2 Surface under Dark and UV Light Irradiation Conditions, J. Phys. Chem. A, 116, 8191–8200, https://doi.org/10.1021/jp305366v, 2012.

Shepherd, J. G. and Working Group on Geoengineering the Climate: Geoengineering the climate: science, governance and uncertainty, RS Policy document 10/09, London, 2009.

Tang, M. J., Telford, P. J., Pope, F. D., Rkiouak, L., Abraham, N. L., Archibald, A. T., Braesicke, P., Pyle, J. A., McGregor, J., Watson, I. M., Cox, R. A., and Kalberer, M.: Heterogeneous reaction of N_2O_5 with airborne TiO_2 particles and its implication for stratospheric particle injection, Atmos. Chem. Phys., 14, 8233–8234, https://doi.org/10.5194/acp-14-8233-2014, 2014.

Tang, M., Keeble, J., Telford, P. J., Pope, F. D., Braesicke, P., Griffiths, P. T., Abraham, N. L., McGregor, J., Watson, I. M., Cox, R. A., Pyle, J. A., and Kalberer, M.: Heterogeneous reaction of $ClONO_2$ with TiO_2 and SiO_2 aerosol particles: implications for stratospheric particle injection for climate engineering, Atmos. Chem. Phys., 16, 15397–15412, https://doi.org/10.5194/acp-16-15397-2016, 2016.

Textor, C., Schulz, M., Guibert, S., Kinne, S., Balkanski, Y., Bauer, S., Berntsen, T., Berglen, T., Boucher, O., Chin, M., Dentener, F., Diehl, T., Easter, R., Feichter, H., Fillmore, D., Ghan, S., Ginoux, P., Gong, S., Grini, A., Hendricks, J., Horowitz, L., Huang, P., Isaksen, I., Iversen, I., Kloster, S., Koch, D., Kirkevåg, A., Kristjansson, J. E., Krol, M., Lauer, A., Lamarque, J. F., Liu, X., Montanaro, V., Myhre, G., Penner, J., Pitari, G., Reddy, S., Seland, Ø., Stier, P., Takemura, T., and Tie, X.: Analysis and quantification of the diversities of aerosol life cycles within AeroCom, Atmos. Chem. Phys., 6, 1777–1813, https://doi.org/10.5194/acp-6-1777-2006, 2006.

Thornton, J. and Abbatt, J. P. D.: Measurements of HO_2 uptake to aqueous aerosol: Mass accommodation coefficients and net reactive loss, J. Geophys. Res.-Atmos., 110, D08309, https://doi.org/10.1029/2004jd005402, 2005.

Thornton, J. A., Jaeglé, L., and McNeill, V. F.: Assessing known pathways for HO_2 loss in aqueous atmospheric aerosols: Regional and global impacts on tropospheric oxidants, J. Geophys. Res.-Atmos., 113, D05303, https://doi.org/10.1029/2007jd009236, 2008.

Usher, C. R., Michel, A. E., Stec, D., and Grassian, V. H.: Laboratory studies of ozone uptake on processed mineral dust, Atmos. Environ., 37, 5337–5347, https://doi.org/10.1016/j.atmosenv.2003.09.014, 2003.

Versick, S., Stiller, G. P., von Clarmann, T., Reddmann, T., Glatthor, N., Grabowski, U., Hoepfner, M., Kellmann, S., Kiefer, M., Linden, A., Ruhnke, R., and Fischer, H.: Global stratospheric hydrogen peroxide distribution from MIPAS-Envisat full resolution spectra compared to KASIMA model results, Atmos. Chem. Phys., 12, 4923–4933, https://doi.org/10.5194/acp-12-4923-2012, 2012.

Visioni, D., Pitari, G., and Aquila, V.: Sulfate geoengineering: a review of the factors controlling the needed injection of sulfur dioxide, Atmos. Chem. Phys., 17, 3879–3889, https://doi.org/10.5194/acp-17-3879-2017, 2017.

Wennberg, P. O., Cohen, R. C., Stimpfle, R. M., Koplow, J. P., Anderson, J. G., Salawitch, R. J., Fahey, D. W., Woodbridge, E. L., Keim, E. R., Gao, R. S., Webster, C. R., May, R. D., Toohey, D. W., Avallone, L. M., Proffitt, M. H., Loewenstein, M., Podolske, J. R., Chan, K. R., Wofsy, S. C.: Removal of stratospheric O_3 by radicals – in situ measurements of OH, HO_2, NO, NO_2, ClO, and BrO, Science, 266, 398–404, https://doi.org/10.1126/science.266.5184.398, 1994.

Winiberg, F. A. F., Smith, S. C., Bejan, I., Brumby, C. A., Ingham, T., Malkin, T. L., Orr, S. C., Heard, D. E., and Seakins, P. W.: Pressure-dependent calibration of the OH and HO_2 channels of a FAGE HO_x instrument using the Highly Instrumented Reactor for Atmospheric Chemistry (HIRAC), Atmos. Meas. Tech., 8, 523–540, https://doi.org/10.5194/amt-8-523-2015, 2015.

Yamamoto, S., Bluhm, H., Andersson, K., Ketteler, G., Ogasawara, H., Salmeron, M., and Nilsson, A.: In situ x-ray photoelectron spectroscopy studies of water on metals and oxides at ambient conditions, J. Phys.-Condes. Matter, 20, 184025, https://doi.org/10.1088/0953-8984/20/18/184025, 2008.